Supporting material

M. Maraldi[1], C. Valero[2], K. Garikipati[1,3,*]

[1]Department of Mechanical Engineering, University of Michigan
[2]M2BE, Aragón Institute of Engineering Research (I3A), University of Zaragoza
[3]Department of Mathematics, University of Michigan

1 Additional details on the model

1.1 Constitutive relations for the chemical potentials and the mechanical forces

The expressions for the chemical potentials are:

$$\mu^{\mathrm{sf}}_{\mathrm{cyt}} = H^{\mathrm{sf}}_{\mathrm{cyt}} + k_B T \ln\left[\widehat{N}_{\mathrm{sf}}/\left(N^{\max}_{\mathrm{sf}} - \widehat{N}_{\mathrm{sf}}\right)\right] \tag{1a}$$

$$\mu_{\mathrm{sf}} = \frac{1}{2}\frac{\left(P x^0_{\mathrm{sf}}\right)^2}{E_{\mathrm{sf}} N^2_{\mathrm{sf}} V_{\mathrm{act}}} + U^{\mathrm{conf}}_{\mathrm{sf}} - \frac{P}{N_{\mathrm{fil}}}\, d_{\mathrm{sf}}. \tag{1b}$$

$$\mu^{\mathrm{fa}}_{\mathrm{cyt}} = H^{\mathrm{fa}}_{\mathrm{cyt}} + k_B T \ln\left[\widehat{N}_{\mathrm{fa}}/\left(N^{\max}_{\mathrm{fa}} - \widehat{N}_{\mathrm{fa}}\right)\right] \tag{1c}$$

$$\mu^{\mathrm{d}}_{\mathrm{fa}} = \frac{1}{2}\frac{P^2 h}{\overline{E}_{\mathrm{fa}} c^{\max}_{\mathrm{fa}} \hat{x}^2_{\mathrm{fa}} b} + \frac{1}{2} B\kappa^2\lambda + U^{conf}_{\mathrm{fa}} - P\left(d_{\mathrm{fa}} + \frac{\lambda}{2}\right) \tag{1d}$$

$$\mu^{\mathrm{p}}_{\mathrm{fa}} = \frac{1}{2}\frac{P^2 h}{\overline{E}_{\mathrm{fa}} c^{\max}_{\mathrm{fa}} \hat{x}^2_{\mathrm{fa}} b} + \frac{1}{2} B\kappa^2\lambda + U^{conf}_{\mathrm{fa}} - P\left(d_{\mathrm{fa}} - \frac{\lambda}{2}\right). \tag{1e}$$

The expressions for the constitutive equations that relate the force to the stress fiber stretch, the focal adhesion deformation and the micropost displacement are:

$$P_{\mathrm{sf}} = \pi r^2_{\mathrm{sf}} E_{\mathrm{sf}} \left[\gamma_{\mathrm{e}}\left(\frac{x_{\mathrm{sf}}}{x^0_{\mathrm{sf}}} - 1\right) + \gamma_{\mathrm{ve}} \int_0^t \frac{\dot{x}_{\mathrm{sf}}(s)}{x^0_{\mathrm{sf}}} e^{-(t-s)/\tau}\, ds\right] + \underbrace{\frac{P^{\mathrm{stl}}_{\mathrm{sf}}}{\dot{\varepsilon}^{\mathrm{con}}}\left(\dot{\varepsilon}^{\mathrm{con}} - \frac{\dot{x}_{\mathrm{sf}}}{x^0_{\mathrm{sf}}}\right)}_{P^{\mathrm{ac}}_{\mathrm{sf}}} \tag{2a}$$

$$P_{\mathrm{fa}} = \frac{\overline{E}_{\mathrm{fa}} \hat{x}_{\mathrm{fa}} b}{h} x^{\mathrm{e}}_{\mathrm{fa}} \tag{2b}$$

$$P_{\mathrm{mp}} = \frac{3\pi E_{\mathrm{mp}} r^4_{\mathrm{mp}}}{4 h^3_{\mathrm{mp}}} x_{\mathrm{mp}} \tag{2c}$$

An explanation of all the parameters appearing in Eq. (1) and Eq. (2) can be found in Tab. 1 and in Maraldi and Garikipati (1). We note that the term in square brackets in Eq. (2a) is the standard linear solid viscoelastic model, chosen because it allows full invertibility between force and displacement responses (1). The stress fiber's active contractile force $P^{\mathrm{ac}}_{\mathrm{sf}}$, given by the last term in Eq. (2a), results from the acto–myosin contractile units introduced in Fig. 1 in the Main Text and discussed there. As also explained in the Main Text, the number of acto–myosin contractile units is proportional to N_{sf}, and each unit in the stress fiber is taken to have the same strain rate $\dot{x}_{\mathrm{am}}/x^0_{\mathrm{am}}$, where x_{am} is the deformed (contracted) length, and x^0_{am} the reference length of the unit. The maximum contractile speed of a myosin motor, $\dot{x}^{\mathrm{con}}_{\mathrm{myos}}$ gives the maximum contractile strain rate of the stress fiber: $-\dot{x}^{\mathrm{con}}_{\mathrm{myos}}/x^0_{\mathrm{sf}}$, which we denote as $\dot{\varepsilon}^{\mathrm{con}}$ for brevity. This is a constant in our model. The contractile force generated by a contractile unit is given by

$$P^{\mathrm{ac}}_{\mathrm{am}} = \frac{P^{\mathrm{stl}}_{\mathrm{am}}}{\dot{\varepsilon}^{\mathrm{con}}}\left(\dot{\varepsilon}^{\mathrm{con}} - \frac{\dot{x}_{\mathrm{am}}}{x^0_{\mathrm{am}}}\right) \tag{3}$$

0006-3495/08/09/2624/12 $2.00

The quantity $P^{\mathrm{ac}}_{\mathrm{am}}$ acts as a force per contractile unit length along each actin filament that makes up the stress fiber. The total contractile force in a single actin filament therefore is the sum of the force contributions from the contractile units along its length, and the total contractile force in the stress fiber is the sum of contractile forces in the parallel actin filaments that are bundled together to form the stress fiber. The total contractile force in the stress fiber therefore is $P^{\mathrm{ac}}_{\mathrm{sf}} = P^{\mathrm{ac}}_{\mathrm{am}}\,\beta N_{\mathrm{sf}}$. Here, β is a constant of proportionality. Since all actomyosin units in a stress fiber are taken to have the same strain rate, we can equivalently write $\dot{x}_{\mathrm{sf}}/x^0_{\mathrm{sf}} = \dot{x}_{\mathrm{am}}/x^0_{\mathrm{am}}$. Finally, the additivity of contractile force from the units can be used to define $P^{\mathrm{stl}}_{\mathrm{sf}} = P^{\mathrm{stl}}_{\mathrm{am}}\,\beta N_{\mathrm{sf}}$. These substitutions together with Eq. (3) allow us to write

$$P^{\mathrm{ac}}_{\mathrm{sf}} = \frac{P^{\mathrm{stl}}_{\mathrm{sf}}}{\dot{\varepsilon}^{\mathrm{con}}}\left(\dot{\varepsilon}^{\mathrm{con}} - \frac{\dot{x}_{\mathrm{sf}}}{x^0_{\mathrm{sf}}}\right) \tag{4}$$

as used in Eq. (2a).

1.2 Solution strategy

For a given set of stress fiber stretch $x_{\mathrm{sf}}(t)$, focal adhesion length, centroid position and deformation – $\hat{x}_{\mathrm{fa}}(t)$, $\tilde{x}_{\mathrm{fa}}(t)$ and $x^{\mathrm{e}}_{\mathrm{fa}}(t)$, respectively–, micropost displacement $x_{\mathrm{mp}}(t)$ and externally-applied substrate displacement $x_{\mathrm{lyr}}(t)$ at time t, where the time history $x_{\mathrm{sf}}(s)$ is known $\forall s \leq t$, the force within the system P can be evaluated by assuming mechanical equilibrium (1). The determination of P is essential for calculating the chemical potentials of the focal adhesion, the stress fiber and the cytosol, which are the driving forces for the chemical processes (1) and appear in the rate equations Eqs. (1–3) in the Main Text.

The system of nonlinear ordinary differential equations Eqs.(1–3) is solved by semi-implicit time integration, using a linear-in-time approximation to evaluate the hereditary integral appearing in Eq.(2a). As initial conditions, we specified the initial focal adhesion length $\hat{x}^0_{\mathrm{fa}}$ and the unstretched stress fiber length x^0_{sf}. Assuming that the focal adhesions are initially in the middle of the microposts allows the focal adhesion ends' initial positions x^0_p and x^0_d to be evaluated. Furthermore, we assumed that the stress fiber initially consists of a single filament; this models the minimal precursor system. Under this assumption and given the size of an actin monomer, the initial number of proteins in the stress fiber N^0_{sf} can be evaluated.

2 Time-dependent response of the system in region *FA-c*

The red and the green curves in Fig.1 show the system's dynamics for configurations falling in region *FA-c* and *FA-c′* on the response map in Fig.2 in the Main Text, respectively. Fig.1b shows that both configurations suffer distal end unbinding of the focal adhesion, whereas the proximal end may either continue growing (red curve), or become stationary because it reaches the edge of the micropost (green curve). In the latter case, overall focal adhesion growth slows down (Fig.1*d*), as new protein complexes can only be added at the distal end.

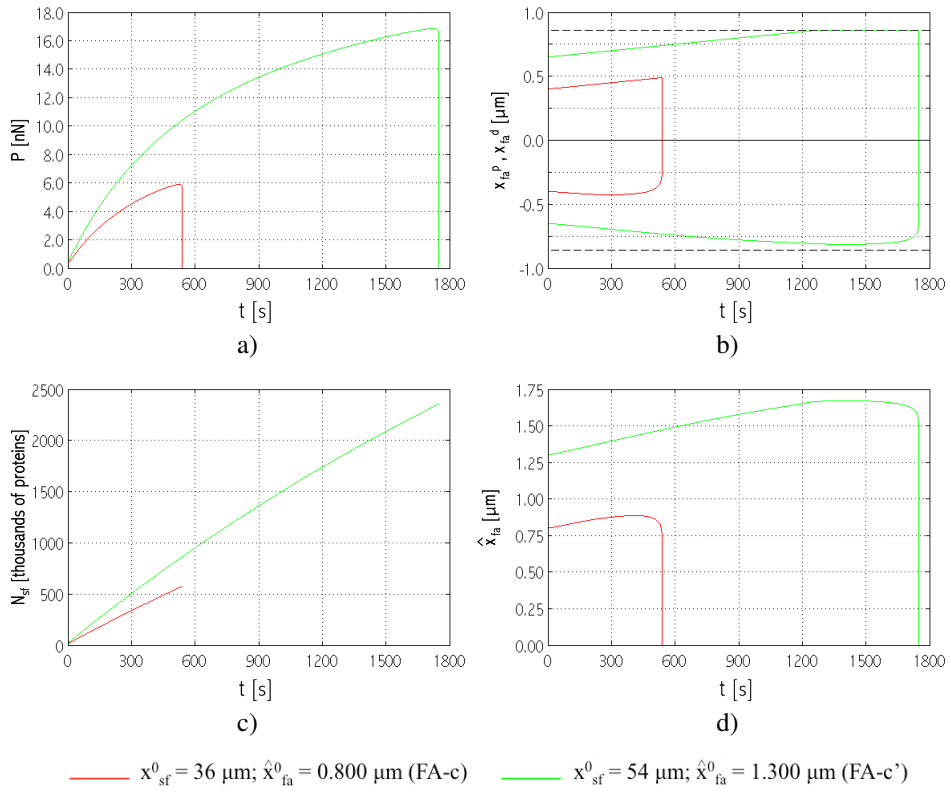

Figure 1: Time evolution of a) force, P; b) focal adhesion distal (initially negative values, $x_{\rm fa}^{\rm d}$) and proximal (positive values, $x_{\rm fa}^{\rm p}$) ends' positions; c) number of actin monomers in the stress fiber, $N_{\rm sf}$; and d) focal adhesion length, $\hat{x}_{\rm fa}$, for two different system initial configurations belonging to region *FA-c* and *FA-c'* in Fig.2 in the Main Text. In b) the dashed black lines indicate the position of the micropost edges.

As P increases (Fig.1a), the term $(\mu_{\rm fa}^{\rm d} - \mu_{\rm cyt}^{\rm fa})$ increases, causing the distal end binding rate to decrease; eventually, $(\mu_{\rm fa}^{\rm d} - \mu_{\rm cyt}^{\rm fa})$ becomes positive, unbinding starts and proceeds at an increasingly higher rate (boosted by the term $\chi_{\rm fa}$, Eq.2). Then, the focal adhesion begins to shrink rapidly, until it is catastrophically resorbed (Fig.1d). The focal adhesion shrinkage makes P decrease rapidly and, of course, when the focal adhesion is fully resorbed P also vanishes. For the chosen parameter values contributing to the chemical potentials $\mu_{\rm sf}$ and $\mu_{\rm cyt}^{\rm sf}$ in these cases, the stress fiber remains in a growth regime with continual recruitment of proteins (Fig.1c) until the system itself collapses.

3 More details on the dynamics of the stress fiber-focal adhesion system under applied external strain

The response map resulting from our computations and reported in Fig.5 in the Main Text is obtained when the strain is applied to the system at $t = 1800$ s. The extent of regions *FA-c(0.05)*, *FA-c(0.10)* and *FA-c(0.15)* depicted in the map depends upon the time at which the step strain is applied. In our model, in fact, the focal adhesion remains far from equilibrium and if the strain is applied at a later instant in time than that chosen here, it will have grown larger and will be able to sustain greater loads, because its critical force will be greater. As a result, the strain necessary to cause system failure will be greater.

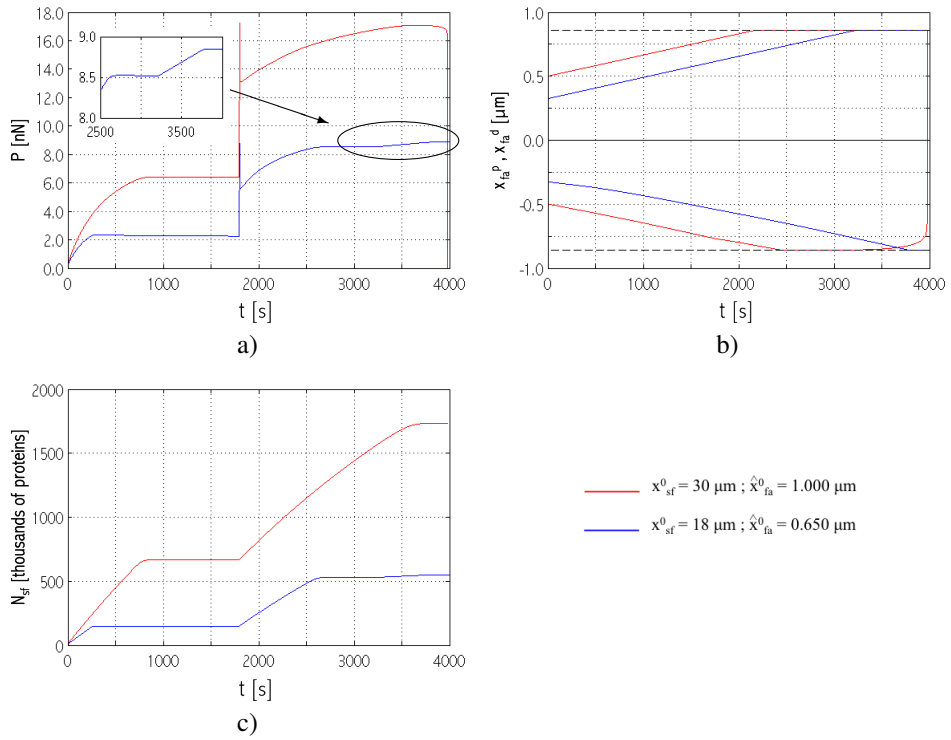

Figure 2: Time evolution of a) force, P; b) focal adhesion distal (initially negative values, $x_{\mathrm{fa}}^{\mathrm{d}}$) and proximal (positive values, $x_{\mathrm{fa}}^{\mathrm{p}}$) ends' positions; and c) number of actin monomers in the stress fiber, N_{sf}, for two different system initial configurations and a step strain $\varepsilon = 0.1$. In b) the dashed black lines indicate the position of the micropost edges.

An equilibrium configuration for the focal adhesion may be attained in some cases if both its end reach the edges of the micropost (blue curves in Fig.2), as discussed in the section pertaining to the time-dependent response of the system with no applied strain in the Main Text. Besides inducing a stiffening effect related to focal adhesion translation away from the stress fiber (as explained in the previous sections and shown in the blue curves in Fig.2), when an external strain is applied to the system and for certain system initial configurations, the presence of a finite cross-section micropost may also cause a more rapid collapse of the system; this case is depicted in Fig.2 (red curves). In both cases, the focal adhesion has grown to cover the cross-section of the micropost; however, if a focal adhesion length equal to the diameter of the micropost is not sufficient to sustain the force within the system (red curves), a rapid failure occurs.

4 Parameters' values

Parameter	Symbol	Value	Unit	Remarks
FA effective elastic modulus	$\overline{E}_{\mathrm{fa}}$	$5.5 \cdot 10^{6}$	Pa	$= E_{\mathrm{fa}}$, elastic modulus assumed to be within the percolation limit (1, 2). E_{fa} estim. for soft, gel-like biological materials
FA width	b	$5.0 \cdot 10^{-7}$	m	Estimate from images in ref. (3) and ref. (4)
FA height	h	$1.0 \cdot 10^{-7}$	m	Rough estimate on the basis of the length of some focal adhesion proteins (5)
Maximum attainable concentration	$c_{\mathrm{fa}}^{\max}$	$1.72 \cdot 10^{7}$	m^{-1}	$= 1/\lambda$
Binding enthalpy	$H_{\mathrm{cyt}}^{\mathrm{fa}}$	0.0	$\mathrm{N} \cdot \mathrm{m}^{2}$	Imposed, focal adhesion does not grow in absence of force (2–4)
Cell membrane curvature	κ	$4.0 \cdot 10^{5}$	m^{-1}	Estimate from cell height $\sim 5\mu\mathrm{m}$.
FA complex length	λ	$5.8 \cdot 10^{-8}$	m	From ref. (6)
Change in internal energy due to binding conformational changes	$U_{\mathrm{fa}}^{\mathrm{conf}}$	0.0	J	Imposed, focal adhesion does not grow in absence of force (2–4)
Equivalent displacement due to binding conformational changes	d_{fa}	$2.9006 \cdot 10^{-8}$	m	Set to reproduce a variety of observed experimental behaviors
Chemical potential of FA proteins in the cytosol	$\mu_{\mathrm{cyt}}^{\mathrm{fa}}$	0.0	J	Imposed, focal adhesion does not grow in absence of force (2–4)
FA proteins binding rate	$k_{\mathrm{fa}}^{\mathrm{b}}$	$2.85 \cdot 10^{-3}$	s^{-1}	Set to reproduce a variety of observed experimental behaviors
FA proteins unbinding rate	$k_{\mathrm{fa}}^{\mathrm{u}}$	$7.98 \cdot 10^{-4}$	s^{-1}	Set to reproduce a variety of observed experimental behaviors
SF Young's modulus	E_{sf}	$8.0 \cdot 10^{7}$	Pa	Estimate based on ref. (7)
Actin monomer volume	V_{act}	$1.047 \cdot 10^{-25}$	m^{3}	Calculated from data on actin length and diameter in ref. (8)
Equivalent displacement due to binding conformational changes	d_{sf}	$2.32 \cdot 10^{-9}$	m	Set to reproduce a variety of observed experimental behaviors
Actin monomer length	L_{actmon}	$2.72 \cdot 10^{-9}$	m	From ref. (8)
Change in internal energy due to binding conformational changes	$U_{\mathrm{sf}}^{\mathrm{conf}}$	0.0	J	Absorbed into $H_{\mathrm{cyt}}^{\mathrm{sf}}$
Binding enthalpy	$H_{\mathrm{cyt}}^{\mathrm{sf}}$	$-2.47 \cdot 10^{-19}$	J	Set to reproduce a variety of observed experimental behaviors
Maximum SF proteins concentration	$c_{\mathrm{sf}}^{\max}$	$1.144 \cdot 10^{11}$	m^{-1}	Estim. from total number of actin monomers in yeast cytosol (9), ratio of volume of cell to yeast cell and considering 50 SFs with mean length of $10\mu\mathrm{m}$ in a cell
SF proteins binding rate	$k_{\mathrm{sf}}^{\mathrm{b}}$	$2.725 \cdot 10^{-4}$	s^{-1}	Adapted from association rate for ATP-actin at the barbed end (10)
SF proteins unbinding rate	$k_{\mathrm{sf}}^{\mathrm{u}}$	0.8	s^{-1}	Adapted from association rate for ATP-actin at the pointed end (10)
Non-dimensional modulus (elastic branch)	γ_{e}	0.9		Set to reproduce a variety of observed experimental behaviors
Non-dimensional modulus (viscoelastic branch)	γ_{ve}	0.1		Set to reproduce a variety of observed experimental behaviors
Relaxation time	τ	10.0	s	Estimate from Fig. 3 in ref. (11)
SF maximum contractile velocity	$\dot{x}_{\mathrm{myos}}^{\mathrm{con}}$	$-5.0 \cdot 10^{-7}$	$\mathrm{m} \cdot \mathrm{s}^{-1}$	From ref. (12)
Myosin stalling force	$P_{\mathrm{myos}}^{\mathrm{stl}}$	$3.0 \cdot 10^{-11}$	N	From ref. (9)
Myosin-to-actin proteins ratio	β	$1.08 \cdot 10^{-3}$		From ref. (9)
Micropost Young's modulus	E_{mp}	$2.5 \cdot 10^{6}$	Pa	From ref. (13)
Micropost radius	r_{mp}	$9.15 \cdot 10^{-7}$	m	From ref. (13)
Micropost height	h_{mp}	$8.3 \cdot 10^{-6}$	m	From ref. (13)
Boltzmann's constant	k_{B}	$1.381 \cdot 10^{-23}$	$\mathrm{J} \cdot \mathrm{K}^{-1}$	
Test temperature	T	310.0	K	

Table 1: Parameters values used in the computations.

Supporting References

1. Maraldi, M., Garikipati, K. (2013). "The chemo-mechanics of cytoskeletal force generation." Submitted.
2. Olberding, J., Thouless, M., Arruda, E., Garikipati, K. (2010). "The non-equilibrium thermodynamics and kinetics of focal adhesion dynamics." PLoS One, 4, e12043.
3. Balaban, N., Schwarz, U., Riveline, D., Goichberg, P., Tzur, G., Sabanay, I., et al. (2001). "Force and focal adhesion assembly: A close relationship studied using elastic micropatterned substrates." Nat. Cell Biol., 3, 466-473.
4. Riveline, D., Zamir, E., Balaban, N., Schwarz, U., Ishikazi, T., Narumiya, S., et al. (2001). "Externally applied local mechanical force induces growth of focal contacts by an mdia1-dependent and rock-independent mechanism." J. Cell Biol., 153, 1175-1185.
5. Zamir, E., Geiger, B. (2001). "Molecular complexity and dynamics of cell-matrix adhesions." J. Cell Sci., 114, 3583-3590.
6. Arnold, M., Cavalcanti-Adam, E.A., Glass, R., Blummel, J., Eck, W., et al. (2004) "Activation of integrin function by nanopatterned adhesive interfaces." ChemPhysChem., 5, 383–388.
7. Deguchi, S., Ohashi, T., Sato, M. (2006). "Tensile properties of single stress fibers isolated from cultured vascular smooth muscle cells." J. Biomech., 39, 2603–2610.
8. Howard, J., "Mechanics of Motor Proteins and the Cytoskeleton." Sinauer Associates, Sunderland Mass. (2001).
9. Wu, J.-Q., Pollard, T. (2005). "Counting cytokinesis proteins globally and locally in fission yeast." Science, 310, 310-314.
10. Pollard, T., Borisy, G. (2003). "Cellular motility driven by assembly and disassembly of actin filaments." Cell, 112, 453-465.
11. Kumar, S., Maxwell, I., Heisterkamp, A., Polte, T., Lele, T., Salanga, M., et al. (2006). "Viscoelastic relaxation of single living stress fibers and its impact on cell shape, cytoskeletal organization, and extracellular matrix mechanics." Biophys. J., 90, 3762-3773.
12. Lord, M., Pollard, T.D. (2004). "UCS protein Rng3p activates actin filament gliding by fission yeast myosin-II" J. Cell Biol., 167 (2), 315–325.
13. Mann, J., Lam, R., Weng, S., Sun, Y., Fu, J. (2012). "A silicone–based stretchable micropost array membrane for monitoring live–cell subcellular cytoskeletal response." Lab Chip, 12, 731–740.